Research Square

Preprints are preliminary reports that have not undergone peer review.
They should not be considered conclusive, used to inform clinical practice,
or referenced by the media as validated information.

ANXA3 Knockdown Attenuated Neurological Deficits and Neuronal Apoptosis after Subarachnoid Hemorrhage via the ATF2/NF-κB Pathway

Yuxiao Meng
First Affiliated Hospital of Harbin Medical University
Jinshuo Yang
Chinese Academy of Medical Sciences & Peking Union Medical College
Xi-ao Wang
First Affiliated Hospital of Harbin Medical University
Shuai Lan:
First Affiliated Hospital of Harbin Medical University
Pei Wu
First Affiliated Hospital of Harbin Medical University
Yuchen Li
First Affiliated Hospital of Harbin Medical University
Huaizhang Shi
huaizhangshi@163.com

First Affiliated Hospital of Harbin Medical University

Research Article

Keywords: Subarachnoid hemorrhage, ANXA3, Neuronal apoptosis, Neurological Deficits, Axonal injury

Posted Date: June 1st, 2026

DOI: https://doi.org/10.21203/rs.3.rs-9759330/v1

License: This work is licensed under a Creative Commons Attribution 4.0 International License.
Read Full License

Additional Declarations: No competing interests reported.

Abstract

Background and purpose

Poor prognosis in patients with subarachnoid hemorrhage (SAH) is largely attributed to neuronal apoptosis. Annexin A3 (ANXA3), a member of the annexin family, orchestrates diverse cellular functions, including exocytosis, cytoskeletal regulation, and membrane trafficking. However, the role of ANXA3 in SAH and its underlying mechanisms remain elusive. The goal of this study was to elucidate the function of ANXA3 in SAH, specifically focusing on its involvement in neuronal apoptosis and the associated molecular mechanisms in both in vivo (rat) and in vitro SAH models.

Methods

In vivo and in vitro SAH models were established via endovascular perforation in rats and oxyhemoglobin induction in HT22 cells, respectively. Western blotting and double immunofluorescence staining were employed to assess ANXA3 expression and its neuronal localization post-SAH. We used neurological scoring, brain water content and blood-brain barrier permeability measurements, terminal deoxynucleotidyl transferase dUTP nick end labeling, immunofluorescence, Morris water maze testing, transmission electron microscopy, and flow cytometry to evaluate pathological and functional outcomes.

Results

Following SAH, ANXA3 expression was significantly upregulated in rat brains. ANXA3 overexpression reduced blood-brain barrier permeability and worsened neurological scores. Furthermore, ANXA3 overexpression exacerbated neuronal apoptosis, evidenced by decreased Bcl-2 levels and increased Bax and cleaved caspase-3 levels. Electron microscopy revealed aggravated axonal injury accompanied by elevated β-Amyloid precursor protein expression. Additionally, levels of phosphorylated activating transcription factor (p-ATF2) and phosphorylated nuclear factor kappa-light-chain-enhancer of activated B cells protein subunit 65 (p-NF-κB p65) were significantly increased. Conversely, ANXA3 knockdown yielded completely opposite results. In vitro experiments mirrored these of vivo findings, suggesting that these effects are potentially mediated via the ANXA3/ATF2/NF-κB signaling pathway.

Conclusion

ANXA3 knockdown ameliorated neurological deficits and mitigated axonal injury following SAH in rats. Furthermore, it attenuated neuronal apoptosis in both in vivo and in vitro models, implicating the ATF2/NF-κB pathway as a contributing mechanism.

Introduction

Subarachnoid hemorrhage (SAH) is a severe subtype of stroke. It ranks third in incidence among all stroke types, and one quarter of patients die before reaching the hospital[1]. The onset of SAH occurs at a relatively young age, with a mean age of approximately 55 years, resulting in the loss of many years of productive life[2]. Among all patients with SAH, approximately 85% have aneurysmal SAH[3]. The concept of early brain injury (EBI) has emerged to describe the acute cerebral damage that occurs immediately following SAH, preceding the development of delayed vasospasm[4]. EBI is currently regarded as the major factor contributing to poor outcomes in patients with SAH, and the secondary injuries it induces include neuroinflammation, blood-brain barrier disruption (BBB), and neuronal apoptosis[5]. However, research on EBI remains insufficient, and more in-depth studies are needed to identify novel therapeutic targets and elucidate its underlying mechanisms to mitigate SAH-induced neurological damage.

Tian et al. recently reported that neuronal apoptosis is a key pathological mechanism underlying SAH-induced brain injury and that it is a major contributor to unfavorable clinical outcomes in patients with SAH[6]. Severe neuronal apoptosis leads to axonal degeneration and structural damage, thereby impairing functions such as axonal transport and axon-dendritic connectivity[7]. Rosenzweig and Carmichael showed that axonal injury and repair mechanisms play a central role in stroke-related damage and recovery, particularly in strokes that occur within the cerebral white matter[8]. Koo et al. found that β-Amyloid precursor protein (β-APP) is transported along the axon via fast anterograde transport and is an extracellular amyloid protein[9]. When an axon is injured, the resulting blockade of axonal transport causes rapid proximal accumulation of β-APP, which is an early and highly sensitive change that makes it a useful marker for detecting axonal injury[10].

Annexins constitute an evolutionarily preserved multigene family of proteins that are capable of binding calcium ions and phospholipids, with widespread expression across both animal and plant species[11]. Annexin A3 (ANXA3) has multiple cellular functions, including exocytotic processes, cytoskeletal modulation, and membrane trafficking[12, 13]. ANXA3 is also closely associated with neurological diseases. Zhou et al. showed that it modulates mechanical allodynia and thermal hyperalgesia in rats, thus highlighting its potential as an important therapeutic target for analgesia[12]. Accumulating evidence indicates that ANXA3 contributes to the pathogenesis of ischemic stroke by exacerbating post-stroke inflammatory responses and that inhibition of ANXA3 confers significant neuroprotective effects in cerebral ischemia/reperfusion injury models[14, 15]. However, whether ANXA3 plays a role in SAH and its underlying mechanisms remain unclear, warranting further in-depth investigation.

Axonal injury is accompanied by dynamic stress-related transcriptional reprogramming in neurons, which is tightly regulated by transcription factor-mediated networks[7]. Although several signaling pathways have been implicated in neuronal apoptosis and axonal injury after SAH, whether additional pathways are involved remains unknown[16]. Activating transcription factor 2 (ATF2) is a multifunctional transcription factor that is regulated at multiple levels and is involved in various developmental and pathological

processes, with roles in controlling cell growth and mediating cellular responses to external stimuli[17]. Increasing evidence indicates that ATF2 plays an important role in neurological disorders. For example, previous studies demonstrated a close association between ATF2 and Alzheimer's disease, in which ATF2 primarily participates in mediating cellular stress responses[18, 19]. Moreover, ATF2 has been shown to play a critical role in ischemic stroke by regulating microglial polarization and modulating neuroinflammatory processes[20].

Zing et al. reported that ANXA3 is closely involved in ATF2 activation and in modulating the expression of downstream target proteins by regulating the phosphorylation status of ATF2[21]. However, the precise mechanisms by which ANXA3 regulates ATF2 phosphorylation to participate in EBI after SAH in rats remain unclear. Similar to ATF2, nuclear factor kappa-light-chain-enhancer of activated B cells (NF-κB) is a transcription factor that is activated in response to inflammatory stimuli after SAH and plays a critical role in the associated pathological processes[22].

Guided by previous investigations and accumulating evidence, the goal of this study was to elucidate the involvement of the ANXA3/ATF2/NF-κB signaling pathway in neuronal apoptosis and axonal injury associated with EBI after SAH. To comprehensively define the mechanistic role of ANXA3 in SAH pathophysiology, both in vivo (rats) and in vitro (HT22 cells) SAH models were systematically established and analyzed.

Materials and Methods

Animals

Adult Sprague-Dawley rats with body weights ranging from 280 to 320 g were were acquired from the Animal Center of the First Affiliated Hospital of Harbin Medical University. All animals were maintained under standardized laboratory conditions, including a controlled relative humidity of approximately 55 ± 5%, a stable ambient temperature of 25–28°C, sufficient air circulation, and a consistent light-dark cycle. Throughout the housing period, rats were allowed ad libitum access to standard chow and water; however, prior to experimental modeling, food and water were withheld for 12 h and 6 h, respectively.All animal experiments were conducted in strict accordance with the guidelines of the National Institutes of Health (NIH) and were approved by the Institutional Animal Care and Use Committee (IACUC) of the First Affiliated Hospital of Harbin Medical University (Approval No. 2024145).

SAH model

The experimental SAH model was established using an intravascular arterial rupture technique adapted from previously published protocols[23]. Briefly, rats were anesthetized with pentobarbital sodium, after which the external and internal carotid arteries were carefully exposed. Through an incision made at the stump of the external carotid artery, a sharpened 4 – 0 monofilament nylon suture was advanced into the

left internal carotid artery until resistance was felt. The filament was left in position momentarily to induce vascular rupture and then promptly withdrawn. Animals in the Sham group underwent identical surgical exposure and filament insertion procedures, except that arterial perforation was not performed.

All experimental protocols involving animals were conducted in strict accordance with the guidelines of the National Institutes of Health and were reviewed and approved by the Animal Ethics Committee of the First Affiliated Hospital of Harbin Medical University in China. Differences between SAH and Sham rats were assessed (See Analytical tests section), and rats from both groups were also used for additional experiments to elucidate the function of ANXA3 in SAH.

Intracerebroventricular injection of adeno-associated virus (AAV)

Rats from the SAH and Sham groups were used to elucidate the function of ANXA3 in SAH. Rats from each group received one of four treatments: an AVV serotype 9 (AAV9) vector encoding annexin A3 (AAV-ANXA3; 1 × 1012 pfu/mL) purchased from Cyagen Biosciences (Guangzhou, China); an AAV9 vector encoding green fluorescent protein (Con-AAV; 1×1012 pfu/mL), which served as the negative control; an AAV9 vector encoding short hairpin RNA (shRNA)-ANXA3 (shRNA-ANXA3; 1 × 1012 pfu/mL); and an AAV9 vector encoding shRNA-Scramble-green fluorescent protein (shRNA-scr; 1 × 1012 pfu/mL). The latter two treatments were used to study the effect of ANXA3 knock down.

Fourteen days prior to SAH induction, rats received stereotaxic injections of 10 μL of AAV-ANXA3, Con-AAV, shRNA-ANXA3, or shRNA-scr into the left lateral ventricle following a previously described protocol[24]. Under deep anesthesia, animals were secured in a stereotaxic frame. Following aseptic preparation and craniotomy, a micro-syringe was lowered to the target coordinates (1.0 mm posterior and 2.0 mm lateral to bregma; 3.5 mm depth from the dural surface). The viral vectors were infused at a rate of 2 μL/min. To prevent backflow, the needle was retained in situ for an additional 15 min post-injection. Rats in the Sham group underwent identical surgical procedures but received an equivalent volume of sterile saline instead of the viral vector.

Experimental design

Experiment 1

To determine the endogenous expression of ANXA3 in the ipsilateral (left) basal temporal lobe cortex, six rats from the SAH and Sham groups were sacrificed at time points of 6, 12, 24, and 72 h post-SAH. Brain tissue was excised and used for western blot analysis to measure the levels of ANXA3. To investigate the colocalization of ANXA3 with neurons, immunofluorescence staining was conducted at 12 h post-operation on tissue samples from both the Sham and SAH groups (n = 3 rats per group). Additionally, SAH grading and transcriptomic sequencing and bioinformatics analysis were performed.

Experiment 2

To evaluate the effects of ANXA3 on neurological outcome, BBB disruption, and long-term cognitive function, rats were randomly assigned to the following six groups: Sham, SAH + Vehicle (phosphate buffered saline), SAH + shRNA-scr, SAH + shRNA-ANXA3, SAH + Con-AAV, and AAV-ANXA3 (n = 12 rats per group). All agents were delivered through stereotaxic intracerebroventricular injection. The modified Garcia scoring system, Evans blue extravasation, Beam balance test, and Morris water maze test were adopted for assessments.

Experiment 3

To investigate the specific role of ANXA3 and the molecular mechanisms related to its effects, rats were randomly divided into Sham, SAH + Vehicle (phosphate buffered saline), SAH + shRNA-scr, SAH + shRNA-ANXA3, SAH + Con-AAV, and SAH + AAV-ANXA3 groups. Western blot(n = 6 rats per group), immunofluorescence(n = 3 rats per group), and transmission electron microscopy (TEM)(n = 3 rats per group) analyses were used.

Experiment 4

To explore the effect of ANXA3 on apoptosis in the vitro SAH model, the following six groups were used: Control, Hemoglobin (Hb) + Vehicle, Hb + shRNA-scr, Hb + shRNA-ANXA3, Hb + Con-AAV, and Hb + AAV-ANXA3. Western blot analysis, immunofluorescence, terminal deoxynucleotidyl transferase dUTP nick end labeling (TUNEL) staining, and flow cytometry were performed. To explore the molecular mechanisms of pathway, Control, Hb + Vehicle, Hb + AAV-ANXA3, and Hb + AAV-ANXA3 + shRNA-ATF2 were used, and western blotting was performed for assessment.

In Vitro SAH model

HT22 cells (Procell, Wuhan, China) derive from immortalized primary mouse hippocampal neurons. For the in vitro SAH model, HT22 cells were incubated at 37°C and 5% CO2 in Dulbecco's modified Eagle's medium (Gibco, Waltham, MA, USA) supplemented with 10% fetal bovine serum (HyClone, Logan, UT, USA) and 1% penicillin and streptomycin (Gibco). Five days post-transfection (AVV), Hb (50 μM) was added to the culture medium to simulate SAH.

Transcriptomic sequencing and bioinformatics analysis

Potential key genes and pathways involved in the pathogenesis of SAH were identified from publicly available transcriptomic datasets retrieved from the Gene Expression Omnibus (GEO) database (https://www.ncbi.nlm.nih.gov/geo/). The GSE36791 dataset provides a transcriptomic profile of peripheral blood cells from patients with aneurysmal subarachnoid hemorrhage.Differential expression analysis was conducted using the limma-voom pipeline in R. Genes with |log2 fold change (log2FC)| ≥ 1 and adjusted p-value < 0.05 were considered differentially expressed genes (DEGs). Volcano plots were generated to visualize global gene expression changes, and heatmaps were constructed to display the

top 18 up- and down-regulated genes ranked by fold change. Functional enrichment analyses, including Gene Ontology (GO) and Kyoto Encyclopedia of Genes and Genomes (KEGG) pathway analyses, were performed using the clusterProfiler R package to identify significantly enriched biological processes and signaling pathways associated with SAH.

Subsequently, transcriptomic analysis was conducted to characterize the alterations in RNA expression in a rat model of SAH (n = 3 biological replicates per group). RNA libraries were constructed with sequencing adapters and sequenced on an Illumina NovaSeq platform. Raw sequencing data were subjected to quality control using FastQC and low-quality reads were filtered. Clean reads were then aligned to the reference genome using HISAT2, and gene expression levels were quantified using featureCounts. Gene Set Enrichment Analysis (GSEA) revealed a significant enrichment of neuroapoptosis-related genes in the SAH group and sham group.

SAH grading

The severity of SAH in rats was independently evaluated by two investigators. At 24 h after SAH induction, rats were anesthetized and euthanized, followed by transcardial perfusion and brain harvesting. The basal surface of the brain was photographed for assessment. The brain base was then divided into six anatomical regions, each of which was scored according to the extent of hemorrhage on a scale of 0–3 using criteria consistent with those described in previous studies[25]. The scores from all regions were summed to obtain the total SAH score for each rat, and animals with a total score < 8 were excluded from subsequent analyses.

Assessment of short-term neurological outcomes post-SAH induction

Neurological function was evaluated 24 h after SAH induction in rats using the modified Garcia scoring system and the beam balance test[26, 27]. The modified Garcia score provides a comprehensive assessment of neurological deficits across multiple behavioral parameters, with individual items scored on a scale of 0–3 or 1–3, yielding a total score ranging from 3 to 18, where higher scores indicate better neurological function. The beam balance test was performed to assess the ability of rats to maintain balance and locomotion on a wooden beam for 1 min, with performance scored from 0 to 4 based on walking distance and the number of falls. All behavioral assessments were conducted independently by two investigators blinded to group allocation, and the median value from three consecutive trials was used for statistical analysis.

Assessment of long-term neurological outcomes post-SAH induction

The Morris water maze test was employed to evaluate learning, memory, and long-term cognitive function in rats and was conducted from days 22 to 28 after SAH induction following previously published protocols[28]. A visible platform trial was performed on day 22, followed by hidden platform

training from days 23 to 27. During the experiments, a circular platform (10 cm in diameter) was submerged approximately 2 cm below the water surface. Each rat underwent three trials per day and was allowed to remain on the platform for 10 s after successfully locating it; animals that failed to find the platform were gently guided to it and maintained there for the same duration. On day 28, a spatial probe trial was conducted in which the platform was removed, and rats were released from a fixed starting point and allowed to swim freely for 120 s. Escape latency, swimming distance, swimming speed, number of platform crossings, and swimming trajectories were recorded and analyzed.

BBB permeability

BBB permeability in the six treatment groups from Experiment 2 was assessed using the Evans blue extravasation method. Briefly, 1 h before sacrifice, rats received an intracardiac injection of 2% Evans blue (Sigma, St. Louis, MO, USA) solution (5 mL/kg) via the left ventricle. The animals were deeply anesthetized and transcardially perfused with ice-cold physiological saline, followed by brain harvesting. Brain tissues were homogenized in 50% trichloroacetic acid and centrifuged to collect the supernatant, which was subsequently mixed with absolute ethanol and trichloroacetic acid and incubated overnight at 4°C in the dark. Evans blue content was quantified by measuring absorbance at 630 nm, which reflected changes in BBB permeability.

TUNEL staining

TUNEL staining was employed to detect cellular apoptosis. Brain sections of rats from Experiment 4 were processed in strict accordance with the manufacturer's instructions using an apoptosis detection kit (Roche, Indianapolis, IN, USA), and the number of TUNEL-positive cells was quantified to assess the level of apoptosis. All microscopic images were acquired under blinded conditions using a fluorescence microscope (Leica Microsystems, DMi8, Wetzlar, Germany).

Western blot analysis

Western blotting was performed according to previously established protocols[29]. Approximately 100 mg of brain tissue from the left temporal basal cortex of rats was collected, homogenized, and lysed using radioimmunoprecipitation assay buffer buffer (Beyotime, Shanghai, China) in strict accordance with the manufacturer's instructions. After centrifugation, the supernatant was collected and protein concentrations were determined.

Subsequently, equal amounts of protein were separated by electrophoresis on 7.5–12.5% sodium dodecyl sulfate-polyacrylamide gel electrophoreses gels and subsequently transferred onto polyvinylidene fluoride membranes. The membranes were blocked with 5% skim milk on a shaker for 2 h and then incubated overnight at 4°C on a rocking platform with the following primary antibodies: anti-ANXA3 (1:1000, ab127924, Abcam), anti-β-actin (1:2500, ab8226, Abcam), anti-Bcl-2 (1:500, WL01556, Wanleibio), anti-Bax (1:5000, 60267-1-Ig, Proteintech, Rosemont), anti-cleaved caspase-3 (1:1000, 9664, Cell Signaling Technology), anti-β-APP (1:500, ab32136, Abcam), anti-ATF2 (1:1000, ab239361, Abcam), anti-phospho-ATF2 (1:1000, #24329, Cell Signaling Tech), anti-NF-kB-p65 (1:1000, #8242, Cell Signaling

Tech), and anti-pNF-kB p65 (1:1000, #3033, Cell Signaling Tech). Following primary antibody incubation, membranes were treated with the corresponding secondary antibodies (1:10,000; Invitrogen, Carlsbad) (31430 or 31460) at ambient temperature for 1 h. Protein bands were visualized using an enhanced chemiluminescence detection kit (NCM Biotech, Suzhou, China), and densitometric analysis was performed with ImageJ software (National Institutes of Health, Bethesda, MD, USA).

TEM

Fresh brain tissues from rats from Experiment 3 were fixed overnight in TEM fixative containing 2.5% glutaraldehyde, and ultrathin sections (60 nm) were cut after fixing with gadolinium tetroxide for 2 h. Sections were dehydrated with acetone and stained with uranium acetate. All sections were observed and photographed utilizing a TEM (Carl Zeiss, Thornwood, NY, USA).

Flow cytometry

Apoptosis in samples from Experiment 4 rats and in HT22 cells was evaluated by flow cytometric analysis using an Annexin V–FITC apoptosis detection kit (Beyotime, China) according to established protocols[30]. Cell samples were analyzed on a NovoCyte Express flow cytometer (ACEA Biosciences, San Diego, CA, USA), and data processing was performed using the associated software. Dead cell counts were calculated using the following formula: [Annexin V+ / propidium iodide (PI) + cells/total cells] × 100%.

Statistical Analysis

All quantitative data were processed and analyzed using GraphPad Prism software (version 8.0; GraphPad Software, San Diego, CA, USA). Results are reported as means ± standard deviation (SD). Comparisons between two groups were performed using an unpaired Student's t test. For experiments involving multiple groups, one-way analysis of variance followed by Tukey's multiple-comparison test was applied. Neurological function assessed over time was analyzed using two-way repeated-measures analysis of variance. $P < 0.05$ was considered to indicate statistical significance.

Results

Transcriptomic sequencing and bioinformatics analysis, SAH Model Mortality, grade Score, and temporal expression of ANXA3 in the rats.

Analysis of the GSE36791 dataset indicated that ANXA3 was significantly upregulated in peripheral blood samples from SAH patients(Fig. 1A–C). KEGG pathway enrichment analysis of differentially expressed genes revealed the apoptosis-related pathways associated with SAH (Fig. 1D). Consistently, ANXA3 was found to be upregulated in our own rat transcriptome data (Fig. 1E–F). Enrichment analysis revealed that differentially expressed genes are involved in pathways related to intrinsic apoptotic signaling pathway (Fig. 1G). GSEA further confirmed significant enrichment of the apoptosis pathway in SAH group(Fig. 1H).

A total of 243 rats were enrolled in this study, including 32 rats in the Sham group and 211 rats in the SAH group. No mortality was observed in the Sham group (0/32). In the SAH group, 43 rats died due to severe anesthesia-related complications or excessively severe SAH, yielding an overall mortality rate of 20.38%. In addition, 18 rats with SAH scores < 8 were excluded from subsequent analyses (Fig. 2A). In SAH-model rats, blood clots were primarily distributed around the circle of Willis or on the ventral surface of the brainstem. SAH scores were comparable across all SAH groups, with no statistically significant differences observed (Fig. 2B).

Endogenous ANXA3 expression in the left temporal cortical tissue was examined by western blotting in the Sham group and in the SAH group at 3, 6, 12, 24, and 72 h following SAH. Compared with the Sham group, ANXA3 protein levels increased significantly as early as 12 h after SAH, reached the peak at that time point, and then gradually declined, with expression levels falling below those of the Sham group at 72 h post-SAH (Fig. 2C–D). Double immunofluorescence staining further confirmed that ANXA3 co-localized with neurons in the cerebral cortex (Fig. 2E).

ANXA3 knockdown attenuated neurological deficits and improved long-term cognitive functions in in vivo SAH models

The modified Garcia and beam balance assessments revealed pronounced neurological impairments in the SAH + Vehicle group compared with the Sham group. Notably, ANXA3 knockdown significantly increased both modified Garcia and beam balance scores in the SAH + shRNA-ANXA3 group relative to the SAH + shRNA-scr group, indicating a neuroprotective effect of ANXA3 knockdown. In contrast, rats subjected to ANXA3 overexpression exhibited markedly worse neurological outcomes, as evidenced by significantly lower scores in the SAH + AAV-ANXA3 group compared with the SAH + Con-AAV group (Fig. 3A–B).

Consistent with these findings, Evans blue extravasation assays demonstrated a substantial increase in BBB permeability following SAH. Suppression of ANXA3 effectively attenuated SAH-induced BBB disruption, whereas ANXA3 overexpression further exacerbated BBB permeability compared with the SAH + Con-AAV group (Fig. 3C).

Long-term spatial learning and memory were evaluated using the Morris water maze. During the hidden platform acquisition phase, rats in the SAH + Vehicle group exhibited significantly prolonged escape latencies and total swimming distance on training days 3–5 compared with the Sham group, indicating impaired spatial learning and memory following SAH. In contrast, suppression of ANXA3 expression markedly reduced escape latency and swimming distance and restored performance to levels comparable to those of Sham animals. This result suggests that downregulation of ANXA3 ameliorates SAH-induced long-term cognitive deficits. Conversely, ANXA3 overexpression significantly increased escape latency relative to the SAH + Con-AAV group, indicating aggravated impairment of long-term memory after SAH (Fig. 3D–E).

In the probe trial, excluding locomotor dysfunction as a confounding factor. Compared with Sham controls, SAH + Vehicle rats spent less time in the target quadrant and crossed the former platform location fewer times, reflecting deficits in spatial memory retention. Reduction of ANXA3 expression significantly reversed these changes by increasing both target quadrant duration and platform crossings, which was indicative of improved long-term neurological function. In contrast, ANXA3 overexpression further decreased target quadrant occupancy and platform crossings, suggesting exacerbated long-term cognitive impairment after SAH (Fig. 3F–I).

ANXA3 participates in neuronal apoptosis

Western blot analysis demonstrated that, relative to the Sham group, the SAH + Vehicle group exhibited a marked reduction in the expression of the anti-apoptotic protein Bcl-2, which was accompanied by significant increases in expressions of the pro-apoptotic markers Bax and cleaved caspase-3. Suppression of ANXA3 expression markedly enhanced the levels of Bcl-2 and Bcl-xl while concomitantly reducing Bax and cleaved caspase-3 expressions, thereby attenuating apoptosis and conferring neuroprotection after SAH.

Consistently, compared with the SAH + shRNA-scr group, rats in the SAH + shRNA-ANXA3 group showed significantly elevated Bcl-2 expression and decreased Bax and cleaved caspase-3 levels, indicating a pronounced anti-apoptotic effect following ANXA3 knockdown. In contrast, ANXA3 overexpression resulted in the opposite pattern, with reduced Bcl-2 expression and increased Bax and cleaved caspase-3 levels in the SAH + AAV-ANXA3 group compared with the SAH + Con-AAV group. This result suggests that excessive ANXA3 expression exacerbates neuronal apoptosis after SAH (Fig. 4A–D).

TUNEL staining demonstrated that the number of apoptotic cells was markedly higher in the SAH + Vehicle group than in the Sham group. Additionally, silencing ANXA3 expression significantly reduced apoptosis, whereas AAV-mediated overexpression of ANXA3 exacerbated apoptotic cell apoptosis (Fig. 4E–F).

ANXA3 knockdown attenuated axonal injury via the ANXA3/ATF2/NF-κB signaling pathway

Western blot analyses demonstrated that, relative to the Sham group, the SAH + Vehicle group exhibited markedly increased expression levels of ANXA3, phosphorylated ATF2 (p-ATF2), phosphorylated NF-κB p65 (p-NF-κB p65), and β-APP. Compared with the SAH + shRNA-scr group, silencing ANXA3 significantly reduced the expression of ANXA3, p-ATF2, p-NF-κB p65, and β-APP, whereas ANXA3 overexpression resulted in higher levels of ANXA3, p-ATF2, p-NF-κB p65, and β-APP compared with the SAH + Con-AAV group (Fig. 5A–E).

TEM showed that in the Sham group, the mitochondria, myelin sheath, and microtubules were intact, and the myelinated fibers and non-myelinated fibers were evenly distributed. In the vehicle group, myelin

sheaths exhibited moth-eaten degeneration associated with mitochondrial swelling. These changes were scattered in the SAH + shRNA-ANXA3 group. The SAH + Con-AAV group exhibited myelin lamellar splitting and disintegration, microtubule disruption, and marked mitochondrial swelling (Fig. 5F). In summary, knockdown of ANXA3 attenuated axonal injury after SAH and was associated with neuroprotective outcomes, whereas ANXA3 overexpression had the opposite effect.

ANXA3 knockdown attenuated apoptosis and axonal injury in vitro

Western blot analysis demonstrated that, compared with the control cells, Bax, cleaved caspase-3, and β-APP protein levels were markedly elevated in Hb-stimulated cells. ANXA3 knockdown significantly reduced the expression of these apoptosis- and axonal injury-associated proteins compared with the shRNA-scrambled control, whereas ANXA3 overexpression resulted in higher Bax, cleaved caspase-3, and β-APP levels relative to the Con-AAV group. Moreover, Bcl-2 expression was decreased in cells subjected to Hb conditions compared with control cells. Silencing ANXA3 partially restored Bcl-2 expression, while enforced ANXA3 expression further suppressed Bcl-2 levels compared with the Con-AAV group (Fig. 6A–E).

The flow cytometry results for apoptotic neurons were consistent with the above results (Fig. 6F–G). Double-immunofluorescence staining of cleaved caspase-3 and neurons showed that the percentage of cleaved caspase-3-positive neurons was significantly higher in the SAH + Vehicle group than in the Sham group. Treatment with shRNA-ANXA3 significantly decreased the percentage of cleaved caspase-3-positive neurons in the SAH + shRNA-ANXA3 group compared to the SAH + shRNA-scr group (Fig. 6H–I).

Collectively, these findings indicate that ANXA3 knockdown alleviates Hb-related neuronal apoptosis and axonal injury in vitro, whereas ANXA3 overexpression exerts opposite effects.

The ANXA3/ATF2/NF-κB signaling pathway contributes to neural injury following SAH

Western blotting revealed significantly higher levels of ANXA3, p-ATF2, and p-NF-κB p65 in the Hb + Vehicle group than in the control group. In contrast, ANXA3 knockdown significantly reduced the protein levels of ANXA3, p-ATF2, and p-NF-κB p65 in the Hb + shRNA-ANXA3 group relative to the Hb + shRNA-scr group. Enforced ANXA3 overexpression led to pronounced upregulation of ANXA3, p-ATF2, and p-NF-κB p65 (Fig. 7A–D). Knockdown of ATF2 using shRNA-ATF2 did not reduce the expression of ANXA3 or p-ATF2, but it markedly decreased the level of p-NF-κB (Fig. 7E–H). These findings suggest that ANXA3 exerts its biological effects by promoting ATF2 activation via phosphorylation, which subsequently triggers phosphorylation-dependent activation of the NF-κB signaling pathway.

Discussion

The results of this study suggest that ANXA3 plays a critical role in the pathogenesis of SAH and that suppression of ANXA3 confers significant neuroprotection via the ANXA3/ATF2/NF-κB signaling pathway. We observed rapid and transient upregulation of ANXA3 expression in the basal temporal lobe as early as 3 h after SAH, indicating its involvement in the early injury response. Functionally, knockdown of ANXA3 alleviated both short- and long-term neurological deficits and improved BBB integrity, whereas ANXA3 overexpression abolished these protective effects.

Mechanistically, modulation of ANXA3 expression significantly influenced neuronal apoptosis and axonal injury, as evidenced by alterations in β-APP, Bcl-2, Bax, and cleaved caspase-3 expression as well as TUNEL staining, ultrastructural axonal changes, and flow cytometry results in both in vivo and in vitro SAH models. ANXA3 overexpression enhanced the activation of ATF2 and NF-κB, while ATF2 knockdown attenuated NF-κB phosphorylation, which supports the notion that ANXA3 acts upstream of the ATF2/NF-κB axis. Collectively, these results indicate that the ANXA3/ATF2/NF-κB pathway contributes to neuronal apoptosis and axonal damage during EBI after SAH and that targeting ANXA3 represents a potential therapeutic strategy for mitigating SAH-induced secondary brain injury.

The annexin family is an evolutionarily conserved multigene protein superfamily whose members share a high degree of structural homology while displaying substantial functional divergence. Annexins are unified by their calcium-dependent phospholipid-binding properties. They exhibit widespread distribution across tissues and species and are expressed in all living organisms except for certain unicellular species[31, 32]. Structurally, annexins are defined by a conserved C-terminal core and a variable N-terminal domain, with the core region containing four annexin repeats of approximately 69–80 amino acids each[11]. Based on their evolutionary origins and distribution patterns, annexins are classified into five subgroups (A, B, C, D, and E), which are predominantly expressed in mammals, invertebrates, Mycetozoa, plants, and protists, respectively. Among these, the A subgroup consists of 12 members (annexins A1–A11 and A13) and has been closely associated with the onset and progression of a wide range of human diseases[33].

The human ANXA3 gene is positioned within the 4q13–q22 chromosomal region and encodes a 323-residue soluble protein known as ANXA3[34]. The short N-terminal region of ANXA3 (20 amino acids) regulates phospholipid membrane association and ion permeability. In addition, ANXA3 harbors two functionally relevant tryptophan residues (W5 in the N-terminus and W190 within the IIIA–IIIB loop), both of which modulate interactions with phospholipid membranes and Ca^{2+}[35, 36]. Previous studies have demonstrated that ANXA3 is involved in the pathogenesis of a wide range of diseases. In autoimmune disorders, ANXA3 has been reported to be closely associated with rheumatoid arthritis and systemic lupus erythematosus, suggesting a potential role in immune regulation and inflammatory responses[37]. Moreover, accumulating evidence has linked aberrant ANXA3 expression to the development and progression of multiple malignancies, including prostate, breast, lung, stomach, and colon cancers[38]. Importantly, dysregulation of ANXA3 contributes to tumor growth and invasion but has also been shown to possess significant diagnostic value in various cancers, highlighting its potential utility as a

biomarker[39]. Regarding neurological disorders, Zhang et al. demonstrated that downregulation of ANXA3 in microglia suppresses neuroinflammation and alleviates ischemic stroke[14]. In the current study, ANXA3 expression significantly increased after SAH. Knockdown of ANXA3 attenuated axonal injury and neuronal apoptosis and exerted neuroprotective effects, whereas ANXA3 overexpression aggravated these injuries, indicating that ANXA3 is a key target in SAH.

Neurons are composed of three principal structural components: the soma, axons, and dendrites. In the nervous system, axons are highly specialized neuronal structures that play a central role in information transmission and integration. Beyond conducting potential, axonal geometry and ion channel distribution jointly regulate the timing and precision of signal propagation, while dynamic modulation of axonal activity can further influence synaptic efficacy, underscoring the importance of axons in neural information processing[40]. Sustained axonal conduction relies on efficient transport and energy supply, which are supported by specialized axonal domains and glial interactions. Due to these complex demands, axons are especially vulnerable to dysfunction and play a key role in neurological pathology[41].

Previous studies have demonstrated that axonal injury is closely associated with a variety of neurological disorders, including Alzheimer's disease and traumatic brain injury. In these conditions, axonal damage represents a prominent pathological feature and directly impairs neural signal transmission and network function. Interventions targeting axonal injury have been shown to improve neurological outcomes, suggesting that axonal protection may represent a novel therapeutic target[42–44].

During EBI following SAH in rats, previous studies have demonstrated that white matter axonal injury plays a critical role and that knockdown of the relevant protein can simultaneously alleviate neuronal apoptosis and axonal damage, further suggesting a close association between axonal injury and neuronal apoptosis[10]. The results of our study further confirm that suppression of ANXA3 has a neuroprotective effect, as evidenced by marked reduction in axonal injury and neuronal apoptosis, thereby contributing to the attenuation of EBI after SAH.

ATF2 is a basic leucine zipper transcription factor of the activator protein 1 family. Through dimerization with partners such as JUN, FOS, CREB, and MAF, ATF2 participates in the formation and regulation of the activator protein 1 transcriptional complex[45]. ATF2 modulates a wide range of downstream genes that are implicated in essential biological processes, including cell proliferation, phenotypic transformation, tissue repair, inflammatory responses, and apoptosis[17]. ATF2 contains multiple phosphorylation sites that respond to diverse signaling pathways, allowing differential activation and fine regulation of its downstream functions[46]. NF-κB functions as a key transcriptional regulator that orchestrates a wide range of innate and adaptive immune activities and plays a central role in controlling inflammatory signaling pathways[47]. Previous studies have shown that NF-κB acts as a downstream effector of ATF2 and participates in signaling pathways involved in tumor development and progression[48]. In the present study, we found that inhibition of ANXA3 reduced the expression of both ATF2 and NF-κB, while

suppression of ATF2 also decreased NF-κB expression. These findings suggest that ANXA3 may modulate apoptosis and axonal injury through the ANXA3/ATF2/NF-κB signaling pathway.

This study was the first to systematically investigate the role of ANXA3 in EBI following SAH and to explore its underlying mechanisms. We demonstrated that the ANXA3/ATF2/NF-κB signaling axis is involved in neuronal apoptosis and axonal injury. Nevertheless, several limitations should be acknowledged. First, the present work focused on validation of a single signaling pathway, whereas the biological effects of ANXA3 may have involved additional molecular mechanisms that remain to be identified. Second, given that NF-κB is a key transcription factor in inflammatory responses, our findings also suggest a potential link between ANXA3 and inflammation-related processes. These issues should be addressed in future studies.

Conclusion

In conclusion, our results show that ANXA3 knockdown significantly improves short- and long-term neurological outcomes post-SAH by attenuating apoptosis and axonal damage in both in vivo and in vitro settings. The ANXA3/ATF2/NF-κB signaling pathway is at least partially involved in neuronal apoptosis and axonal injury during SAH. These results suggest that ANXA3 may be a promising therapeutic target for patients with SAH.

Declarations

Conflict of interest

The authors declare that the research was conducted in the absence of any commercial or financial relationships that could be construed as a potential conflict of interest.

Funding

This study was supported by the National Natural Science Foundation, China (82571485, U25A2062), the Natural Science Foundation of Heilongjiang Province of China (YQ2023H008, PL2O24HO55).

Author Contribution

YM, YL and HS: designed and conceived this research. YM, and JY:animal experiments. YM and SL: cell experiments. XW, and PW: data analysis. YM, and JY: prepared the manuscript. PW, YL, and HS : revised the manuscript. YM and JY contributed equally. All authors contributed to manuscript revision, read,and approved the submitted version.

Acknowledgement

The authors gratefully acknowledge the financial support from the National Natural Science Foundation, China (82571485,U25A2062), the Natural Science Foundation of Heilongjiang Province of China (YQ2023H008, PL2O24HO55).

References

1. Claassen J, Park S. Spontaneous subarachnoid haemorrhage. Lancet. 2022;400(10355):846–62. 10.1016/s0140-6736(22)00938-2.
2. Macdonald RL, Schweizer TA. Spontaneous subarachnoid haemorrhage. Lancet. 2017;389(10069):655–66. 10.1016/s0140-6736(16)30668-7.
3. van Gijn J, Kerr RS, Rinkel GJ. *Subarachnoid haemorrhage.* Lancet, 2007. 369(9558): pp. 306 – 18.10.1016/s0140-6736(07)60153-6
4. Fujii M, Yan J, Rolland WB, Soejima Y, Caner B, Zhang JH. Early brain injury, an evolving frontier in subarachnoid hemorrhage research. Transl Stroke Res. 2013;4(4):432–46. 10.1007/s12975-013-0257-2.
5. Tao W, Zhang G, Liu C, Jin L, Li X, Yang S. *Low-dose LPS alleviates early brain injury after SAH by modulating microglial M1/M2 polarization via USP19/FOXO1/IL*-10/IL-10R1 *signaling.* Redox Biol, 2023. 66: p. 102863.10.1016/j.redox.2023.102863
6. Tian Q, Liu C, Liao J, Wang G, Han W, Xiong X, et al. ATF2/BAP1 Axis Mediates Neuronal Apoptosis After Subarachnoid Hemorrhage via P53 Pathway. Stroke. 2024;55(8):2113–25. 10.1161/strokeaha.123.045781.
7. Hopkins BD, Fine B, Steinbach N, Dendy M, Rapp Z, Shaw J, et al. A secreted PTEN phosphatase that enters cells to alter signaling and survival. Science. 2013;341(6144):399–402. 10.1126/science.1234907.
8. Rosenzweig S, Carmichael ST. Age-dependent exacerbation of white matter stroke outcomes: a role for oxidative damage and inflammatory mediators. Stroke. 2013;44(9):2579–86. 10.1161/strokeaha.113.001796.
9. Koo EH, Sisodia SS, Archer DR, Martin LJ, Weidemann A, Beyreuther K, et al. Precursor of amyloid protein in Alzheimer disease undergoes fast anterograde axonal transport. Proc Natl Acad Sci U S A. 1990;87(4):1561–5. 10.1073/pnas.87.4.1561.
10. Chen H, Zhou C, Zheng J, Zhang Z, Deng Y, Cheng C, et al. PTEN and AKT/GSK-3β/CRMP-2 signaling pathway are involved in neuronal apoptosis and axonal injury in early brain injury after SAH in rats. Genes Dis. 2022;9(1):252–67. 10.1016/j.gendis.2020.05.002.
11. Gerke V, Moss SE. Annexins: from structure to function. Physiol Rev. 2002;82(2):331–71. 10.1152/physrev.00030.2001.

12. Zou W, Xu W, Song Z, Zhong T, Weng Y, Huang C, et al. Proteomic Identification of an Upregulated Isoform of Annexin A3 in the Spinal Cords of Rats in a Neuropathic Pain Model. Front Neurosci. 2017;11:484. 10.3389/fnins.2017.00484.
13. Zhang Z, Li Z, Ma Z, Deng M, Xing M, Wu J et al. *Annexin A3 as a Marker Protein for Microglia in the Central Nervous System of Rats.* Neural Plast, 2021. 2021: p. 5575090.10.1155/2021/5575090
14. Zhang Z, Zhang M, Li D, Shu R, Pan Q, Zou W, et al. Microglial Annexin A3 Downregulation Alleviates Ischemic Injury by Inhibiting NF-κB/NLRP3-mediated Inflammation. Inflammation. 2025;48(5):3606–17. 10.1007/s10753-025-02287-4.
15. Min XL, He M, Shi Y, Xie L, Ma XJ, Cao Y. *miR-18b attenuates cerebral ischemia/reperfusion injury through regulation of ANXA3 and PI3K/Akt signaling pathway.* Brain Res Bull, 2020. 161: pp. 55–64.10.1016/j.brainresbull.2020.04.021
16. Zhao Y, Zhao Y, Zhang M, Zhao J, Ma X, Huang T et al. *Inhibition of TLR4 Signalling-Induced Inflammation Attenuates Secondary Injury after Diffuse Axonal Injury in Rats.* Mediators Inflamm, 2016. 2016: p. 4706915.10.1155/2016/4706915
17. Watson G, Ronai ZA, Lau E. ATF2, a paradigm of the multifaceted regulation of transcription factors in biology and disease. Pharmacol Res. 2017;119:347–57. 10.1016/j.phrs.2017.02.004.
18. Yang T, Zhang Y, Chen L, Thomas ER, Yu W, Cheng B, et al. The potential roles of ATF family in the treatment of Alzheimer's disease. Biomed Pharmacother. 2023;161:114544. 10.1016/j.biopha.2023.114544.
19. Vargas DM, De Bastiani MA, Zimmer ER, Klamt F. Alzheimer's disease master regulators analysis: search for potential molecular targets and drug repositioning candidates. Alzheimers Res Ther. 2018;10(1):59. 10.1186/s13195-018-0394-7.
20. Cao X, Pu Y. Curcumin Regulates Microglia Polarization to Alleviate Ischemic Stroke by Targeting microRNA-205-5p/Kruppel-Like Factor 2 (KLF2)/Activating Transcription Factor 2 (ATF2) Axis. Chem Biol Drug Des. 2025;105(1). 10.1111/cbdd.70050. e70050.
21. Xing M, Liang S, Cao W, Guo Q, Zou W. Annexin A3 Represses Endothelial Permeability and Inflammation During Sepsis via Actin Cytoskeleton Modulation. Adv Sci (Weinh). 2025;12(22). 10.1002/advs.202416904. e2416904.
22. Shao J, Meng Y, Yuan K, Wu Q, Zhu S, Li Y, et al. RU.521 mitigates subarachnoid hemorrhage-induced brain injury via regulating microglial polarization and neuroinflammation mediated by the cGAS/STING/NF-κB pathway. Cell Commun Signal. 2023;21(1):264. 10.1186/s12964-023-01274-2.
23. Wu Q, Yuan K, Yao Y, Yao J, Shao J, Meng Y, et al. LAMC1 attenuates neuronal apoptosis via FAK/PI3K/AKT signaling pathway after subarachnoid hemorrhage. Exp Neurol. 2024;376:114776. 10.1016/j.expneurol.2024.114776.
24. Liu N, Li C, Yan C, Yan HC, Jin BX, Yang HR, et al. BCAT1 alleviates early brain injury by inhibiting ferroptosis through PI3K/AKT/mTOR/GPX4 pathway after subarachnoid hemorrhage. Free Radic Biol Med. 2024;222:173–86. 10.1016/j.freeradbiomed.2024.05.045.

25. Yang J, Wu Q, Li Y, Zhang Y, Lan S, Yuan K, et al. BL-918 alleviates oxidative stress in rats after subarachnoid hemorrhage by promoting mitophagy through the ULK1/PINK1/Parkin pathway. Free Radic Biol Med. 2024;224:846–61. 10.1016/j.freeradbiomed.2024.10.261.
26. Okada T, Enkhjargal B, Travis ZD, Ocak U, Tang J, Suzuki H, et al. FGF-2 Attenuates Neuronal Apoptosis via FGFR3/PI3k/Akt Signaling Pathway After Subarachnoid Hemorrhage. Mol Neurobiol. 2019;56(12):8203–19. 10.1007/s12035-019-01668-9.
27. Tian Y, Liu B, Li Y, Zhang Y, Shao J, Wu P, et al. Activation of RARα Receptor Attenuates Neuroinflammation After SAH via Promoting M1-to-M2 Phenotypic Polarization of Microglia and Regulating Mafb/Msr1/PI3K-Akt/NF-κB Pathway. Front Immunol. 2022;13:839796. 10.3389/fimmu.2022.839796.
28. Yuan K, Wu Q, Yao Y, Shao J, Zhu S, Yang J, et al. Deacetylase SIRT2 Inhibition Promotes Microglial M2 Polarization Through Axl/PI3K/AKT to Alleviate White Matter Injury After Subarachnoid Hemorrhage. Transl Stroke Res. 2025;16(4):1075–93. 10.1007/s12975-024-01282-5.
29. Sun B, Li Y, Lan S, Wang XA, Ling Y, Sawant H, et al. Retinoic acid-inducible gene-I aggravates neuroinflammation in early brain injury after subarachnoid hemorrhage through mediating brain microvascular endothelial cell pyroptosis. Neurotherapeutics. 2025;22(4):e00572. 10.1016/j.neurot.2025.e00572.
30. Li Y, Liu Y, Wu P, Tian Y, Liu B, Wang J et al. *Inhibition of Ferroptosis Alleviates Early Brain Injury After Subarachnoid Hemorrhage In Vitro and In Vivo via Reduction of Lipid Peroxidation.* Cell Mol Neurobiol, 2021. 41(2): pp. 263–278.10.1007/s10571-020-00850-1
31. Lizarbe MA, Barrasa JI, Olmo N, Gavilanes F, Turnay J. Annexin-phospholipid interactions. Functional implications. Int J Mol Sci. 2013;14(2):2652–83. 10.3390/ijms14022652.
32. Moss SE, Morgan RO. The annexins. Genome Biol. 2004;5(4):219. 10.1186/gb-2004-5-4-219.
33. Yang L, Lu P, Yang X, Li K, Qu S. Annexin A3, a Calcium-Dependent Phospholipid-Binding Protein: Implication in Cancer. Front Mol Biosci. 2021;8:716415. 10.3389/fmolb.2021.716415.
34. Mussunoor S, Murray GI. The role of annexins in tumour development and progression. J Pathol. 2008;216(2):131–40. 10.1002/path.2400.
35. Sopkova J, Raguenes-Nicol C, Vincent M, Chevalier A, Lewit-Bentley A, Russo-Marie F, et al. Ca(2+) and membrane binding to annexin 3 modulate the structure and dynamics of its N terminus and domain III. Protein Sci. 2002;11(7):1613–25. 10.1110/ps.4230102.
36. Liu C, Li N, Liu G, Feng X. Annexin A3 and cancer. Oncol Lett. 2021;22(6):834. 10.3892/ol.2021.13095.
37. Okada Y, Terao C, Ikari K, Kochi Y, Ohmura K, Suzuki A, et al. Meta-analysis identifies nine new loci associated with rheumatoid arthritis in the Japanese population. Nat Genet. 2012;44(5):511–6. 10.1038/ng.2231.
38. Ozturk A. Role of annexin A3 in breast cancer (Review). Mol Clin Oncol. 2022;16(6):111. 10.3892/mco.2022.2544.

39. Jamaspishvili T, Kral M, Khomeriki I, Student V, Kolar Z, Bouchal J. Urine markers in monitoring for prostate cancer. Prostate Cancer Prostatic Dis. 2010;13(1):12–9. 10.1038/pcan.2009.31.
40. Debanne D, Campanac E, Bialowas A, Carlier E, Alcaraz G. Axon physiology. Physiol Rev. 2011;91(2):555–602. 10.1152/physrev.00048.2009.
41. Dan L, Zhang Z. Alzheimer's disease: an axonal injury disease? Front Aging Neurosci. 2023;15:1264448. 10.3389/fnagi.2023.1264448.
42. Salvadores N, Sanhueza M, Manque P, Court FA. Axonal Degeneration during Aging and Its Functional Role in Neurodegenerative Disorders. Front Neurosci. 2017;11:451. 10.3389/fnins.2017.00451.
43. Jamjoom AAB, Rhodes J, Andrews PJD, Grant SGN. The synapse in traumatic brain injury. Brain. 2021;144(1):18–31. 10.1093/brain/awaa321.
44. Wang KK, Yang Z, Zhu T, Shi Y, Rubenstein R, Tyndall JA, et al. An update on diagnostic and prognostic biomarkers for traumatic brain injury. Expert Rev Mol Diagn. 2018;18(2):165–80. 10.1080/14737159.2018.1428089.
45. Lopez-Bergami P, Lau E, Ronai Z. Emerging roles of ATF2 and the dynamic AP1 network in cancer. Nat Rev Cancer. 2010;10(1):65–76. 10.1038/nrc2681.
46. Gozdecka M, Breitwieser W. The roles of ATF2 (activating transcription factor 2) in tumorigenesis. Biochem Soc Trans. 2012;40(1):230–4. 10.1042/bst20110630.
47. Liu T, Zhang L, Joo D, Sun SC. NF-κB signaling in inflammation. Signal Transduct Target Ther. 2017;2:17023–. 10.1038/sigtrans.2017.23.
48. Zhu ZB, Wu D, Mao C, Gu YP, Zhang J, Fang L, et al. Elevated FBXO45 promotes TFG ubiquitination and drives lung metastasis of hepatocellular carcinoma. JHEP Rep. 2025;7(10):101519. 10.1016/j.jhepr.2025.101519.

Figures

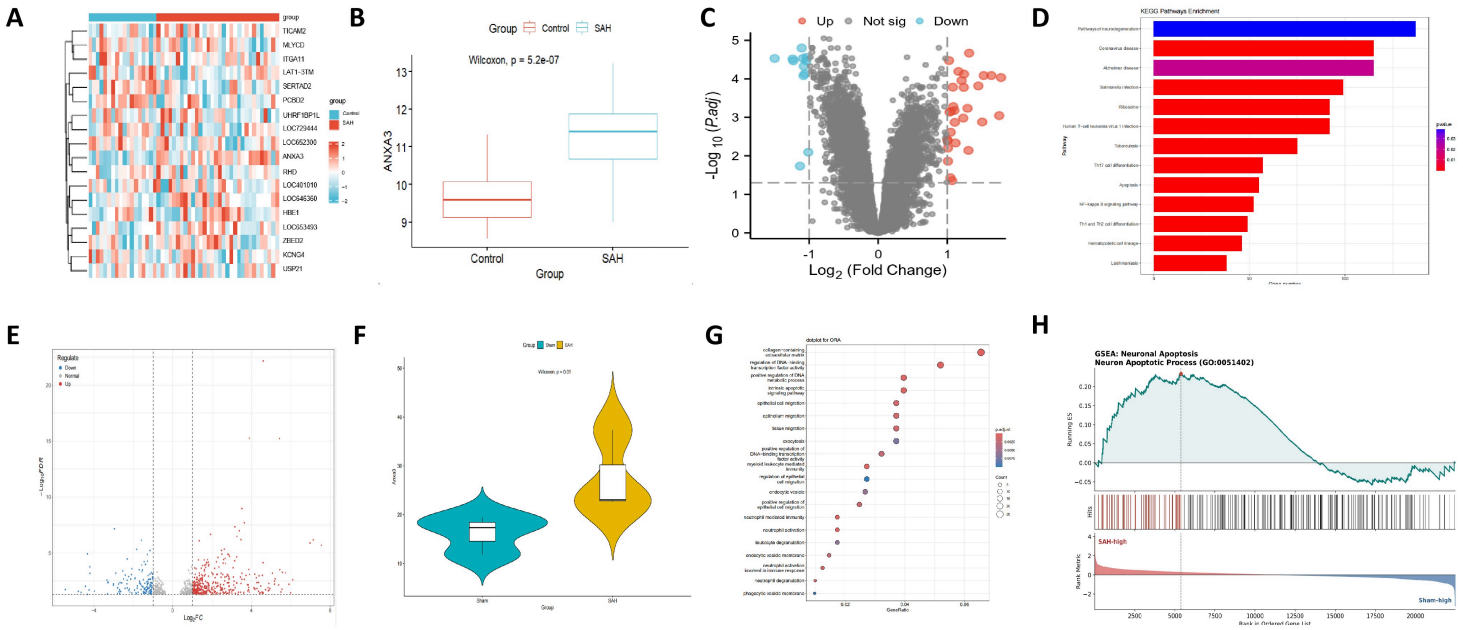
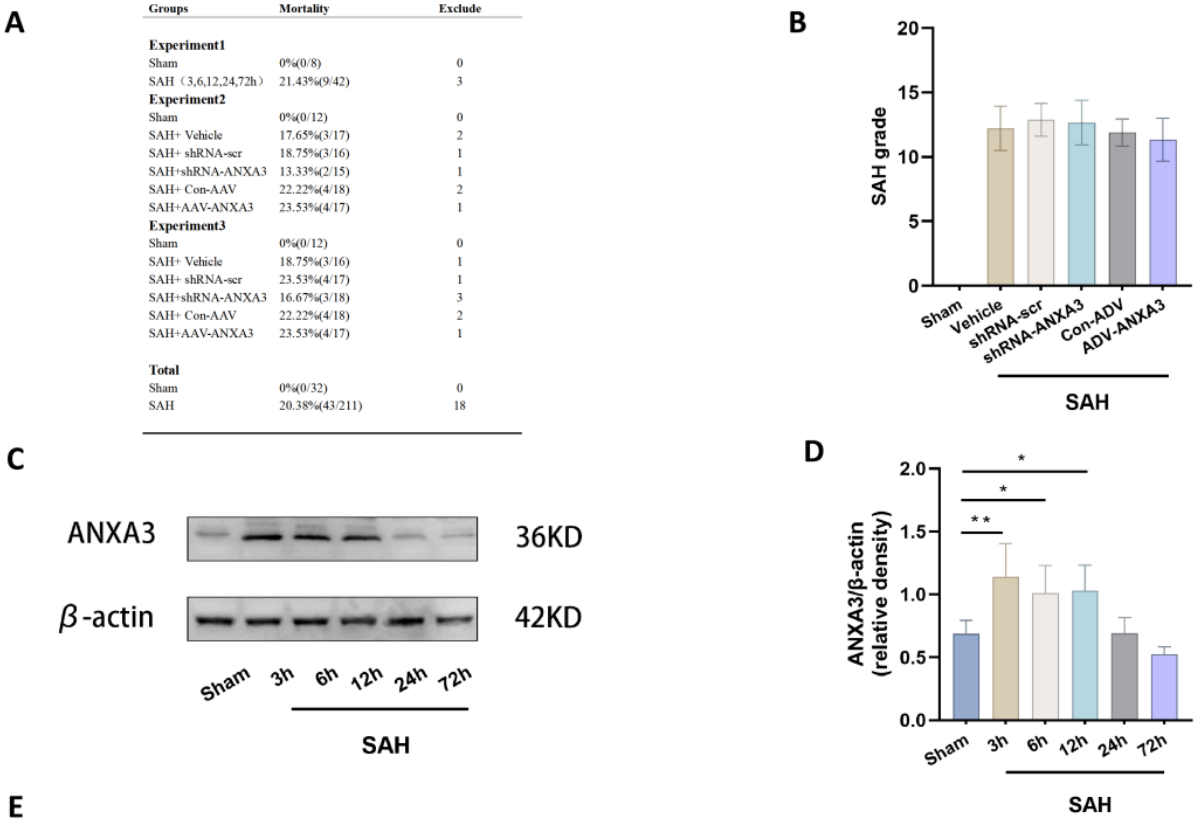


Figure 1

ANXA3 is identified as a potential biomarker for SAH. (A) Heatmap showing the expression profiles of the top 18 differentially expressed genes (DEGs) between the control and SAH groups in GSE36791; (B) Box plot illustrating the expression levels of ANXA3 in the control and SAH groups, with statistical significance assessed by the Wilcoxon test; (C) Volcano plot displaying the distribution of differentially expressed genes between the two groups; (D) KEGG pathway enrichment analysis of DEGs, showing significantly enriched signaling pathways associated with SAH; (E) Volcano plot of the transcriptomic analysis in rats. (n = 3 biological replicates per group). (F) The expression of ANXA3 was elevated in the SAH group; (G) KEGG pathway enrichment analysis shows the activated and suppressed pathways in SAH groups; (H) GSEA demonstrated that neuroapoptosis-associated gene signatures were significantly enriched in the SAH group relative to the sham controls.

A

Groups	Mortality	Exclude
Experiment1		
Sham	0%(0/8)	0
SAH（3,6,12,24,72h）	21.43%(9/42)	3
Experiment2		
Sham	0%(0/12)	0
SAH+ Vehicle	17.65%(3/17)	2
SAH+ shRNA-scr	18.75%(3/16)	1
SAH+shRNA-ANXA3	13.33%(2/15)	1
SAH+ Con-AAV	22.22%(4/18)	2
SAH+AAV-ANXA3	23.53%(4/17)	1
Experiment3		
Sham	0%(0/12)	0
SAH+ Vehicle	18.75%(3/16)	1
SAH+ shRNA-scr	23.53%(4/17)	1
SAH+shRNA-ANXA3	16.67%(3/18)	3
SAH+ Con-AAV	22.22%(4/18)	2
SAH+AAV-ANXA3	23.53%(4/17)	1
Total		
Sham	0%(0/32)	0
SAH	20.38%(43/211)	18



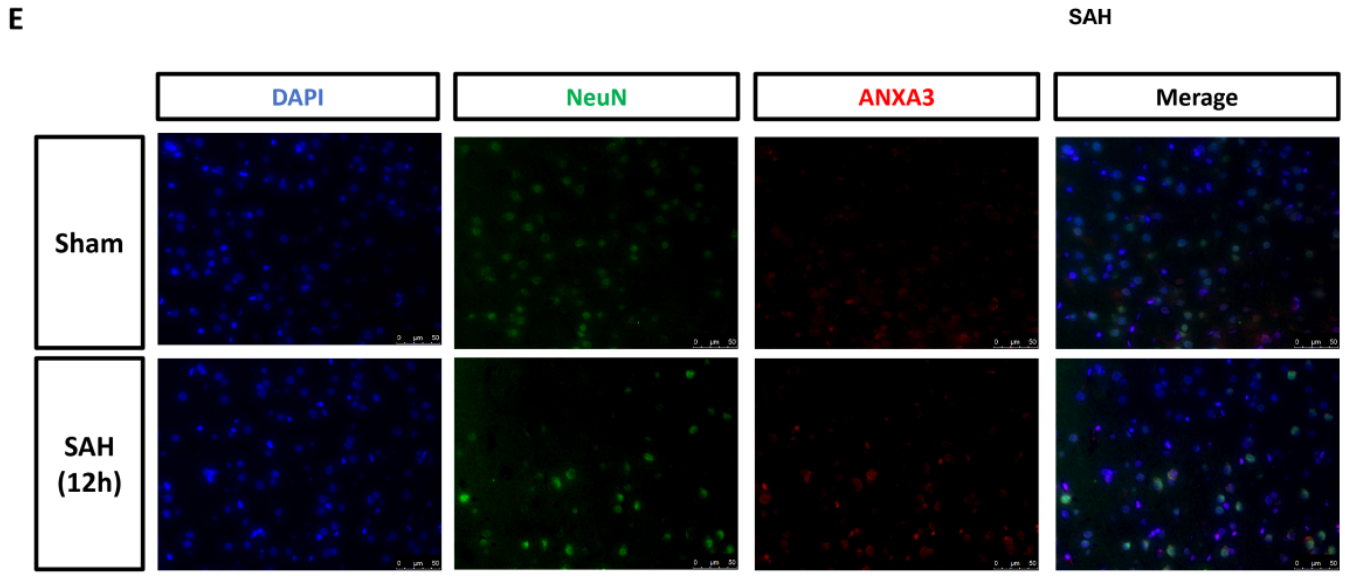


Figure 2

Images of mortality, brain tissues, SAH grading, and temporal expression of ANXA3 in rats. (A) Animal usage and mortality; (B) SAH grading scores in each group; (C–D) Representative western blot bands of time course and quantitative analyses for ANXA3 (n = 6 per group). *P < 0.05 vs. Sham group; **P < 0.01 vs. Sham group; (E) Representative images of double immunofluorescence staining for ANXA3 with neurons at 12 h after SAH (n = 3 per group). Scale bar = 50 mm. Data are shown as means ± SD.

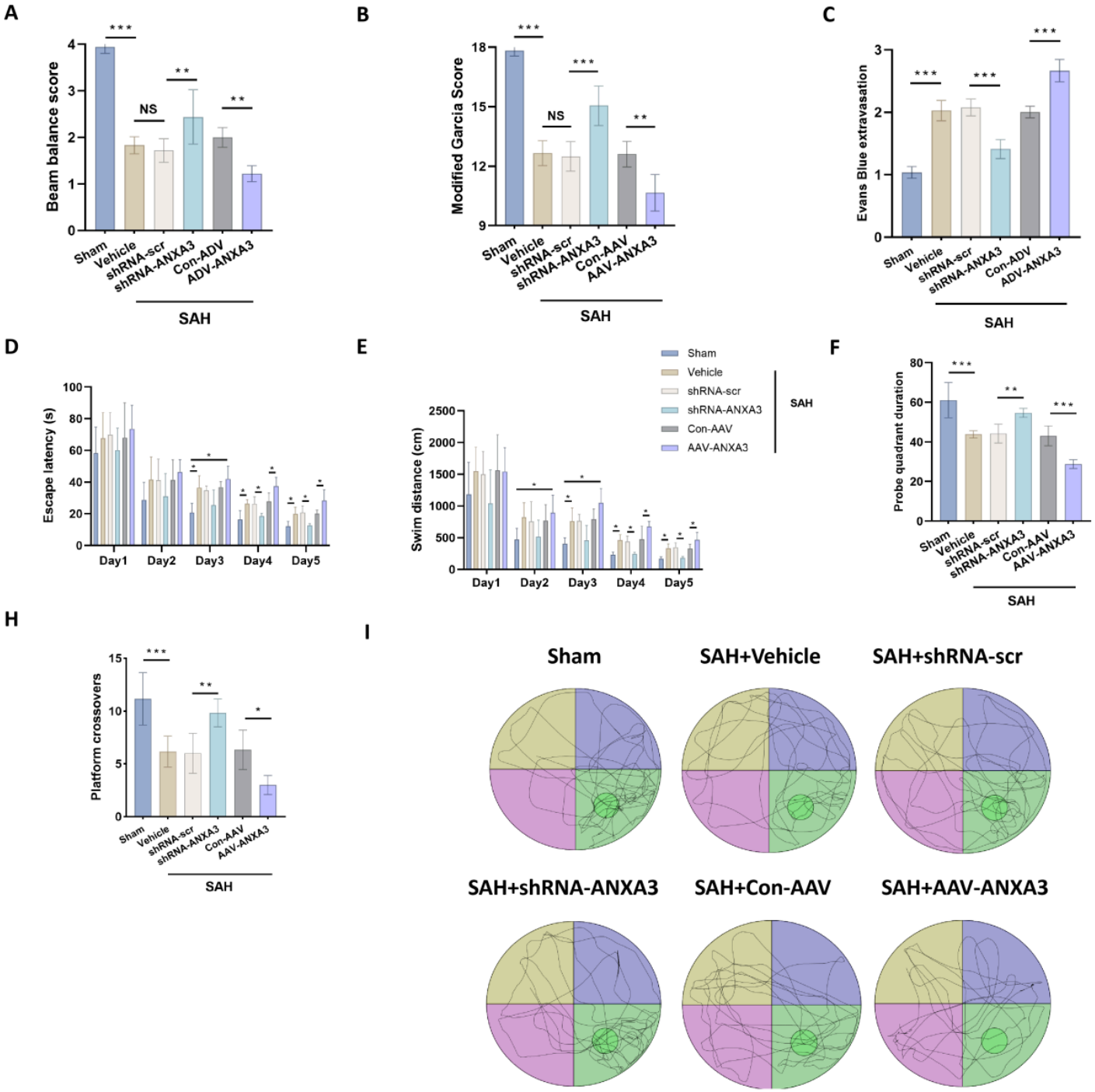


Figure 3

ANXA3 knockdown attenuated neurological deficits and improved long-term cognitive functions in in vivo SAH models. (A–B) The beam balance score and modified Garcia score of rats (n = 6 per group); (C) Evans blue extravasation of the rat brain (n = 6 per group); (D–E) Escape latency and swim distance in the visible platform trial of the water maze test (n = 6 per group); (F–H) Probe quadrant duration and platform crossovers in the probe trial of the water maze test (n = 6 per group); (I) Representative trace of rats in the water maze test (n = 6 per group). Data are shown as means ± SD. *P < 0.05, **P < 0.01, ***P < 0.001.

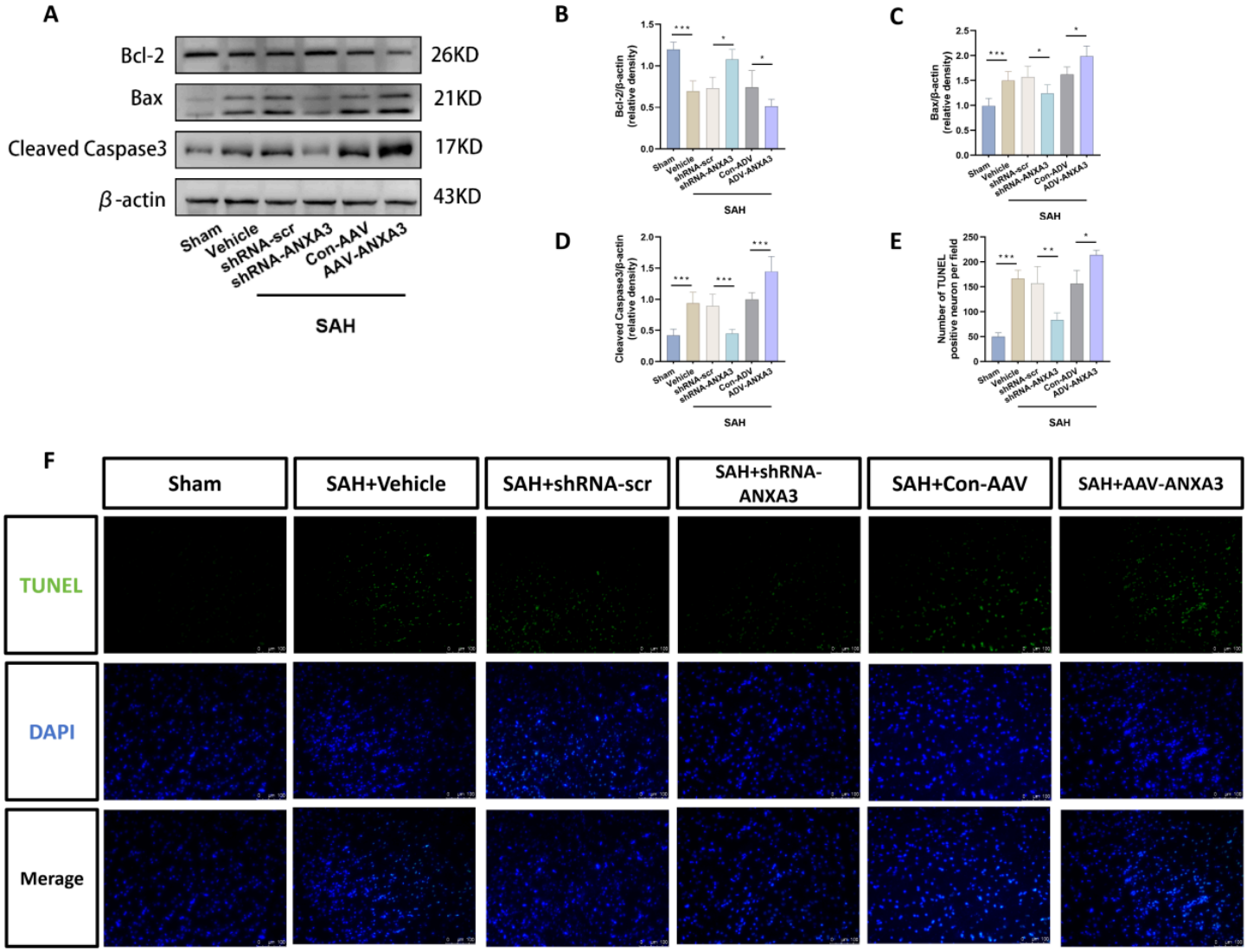


Figure 4

ANXA3 participated in neuronal apoptosis. (A–D) Representative western blot images and densitometric quantification of the expression of Bcl-2, Bax, and cleaved caspase-3 12 h after SAH (n = 6 per group); (E–F) Representative images of TUNEL staining and quantitative analysis of TUNEL-positive neuronal cells (n = 3 per group). Scale bar =100 μm. Data are shown as means ± SD. *P < 0.05, ** P< 0.01, ***P < 0.001.

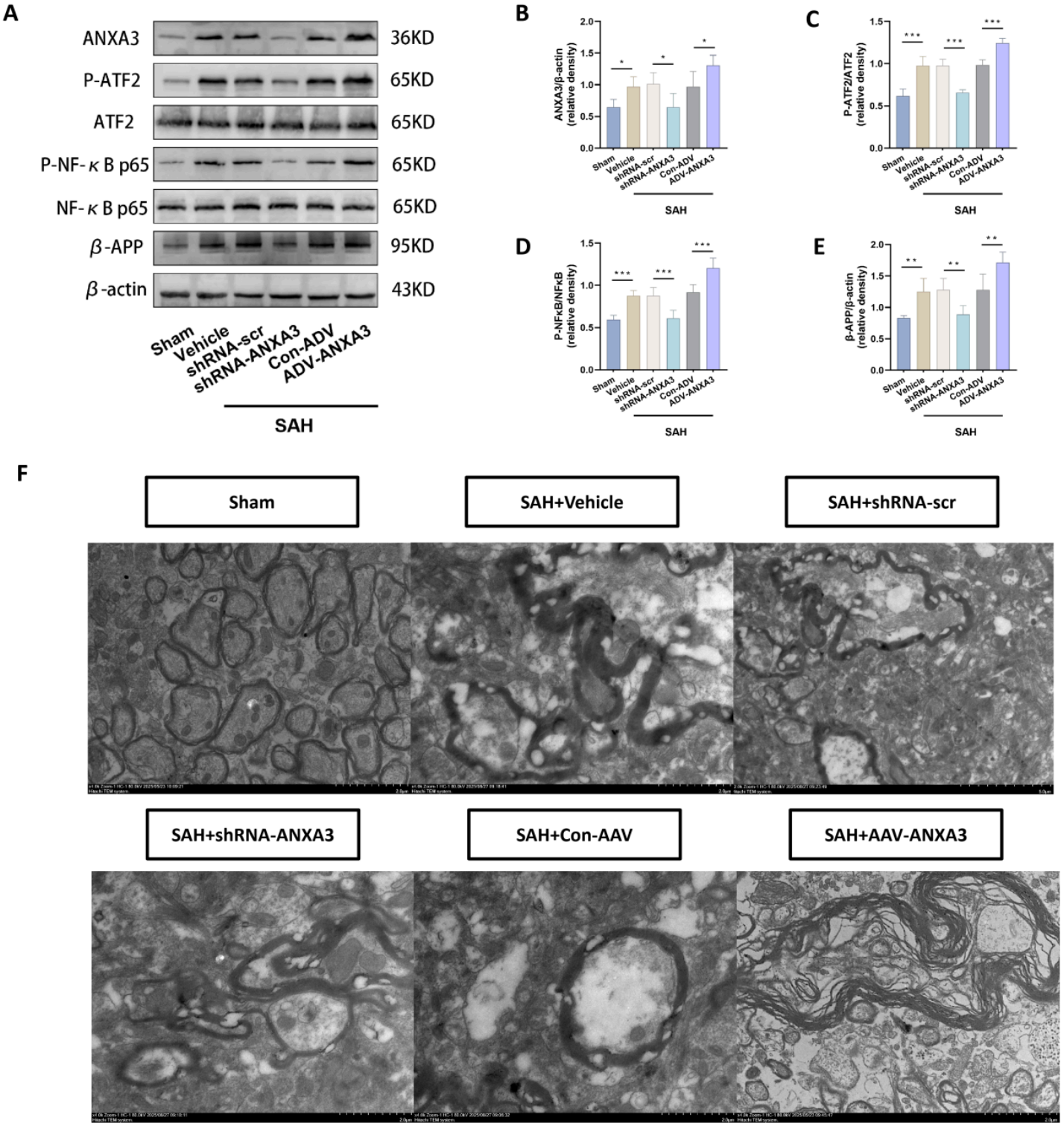


Figure 5

ANXA3 overexpression exacerbated axonal injury via the ANXA3/ATF2/NF-κB signaling pathway. (A–E) Representative western blot images and densitometric quantification of the expression of ANXA3, p-ATF2, ATF2, p-NF-κB p65, NF-κB p65, and β-APP (n = 6 per group); (F) Representative TEM images of brain tissue of rats in each group (n = 3 per group). Scale bar = 2 μm. Data are shown as means ± SD. *P< 0.05, **P < 0.01, *** P < 0.001.

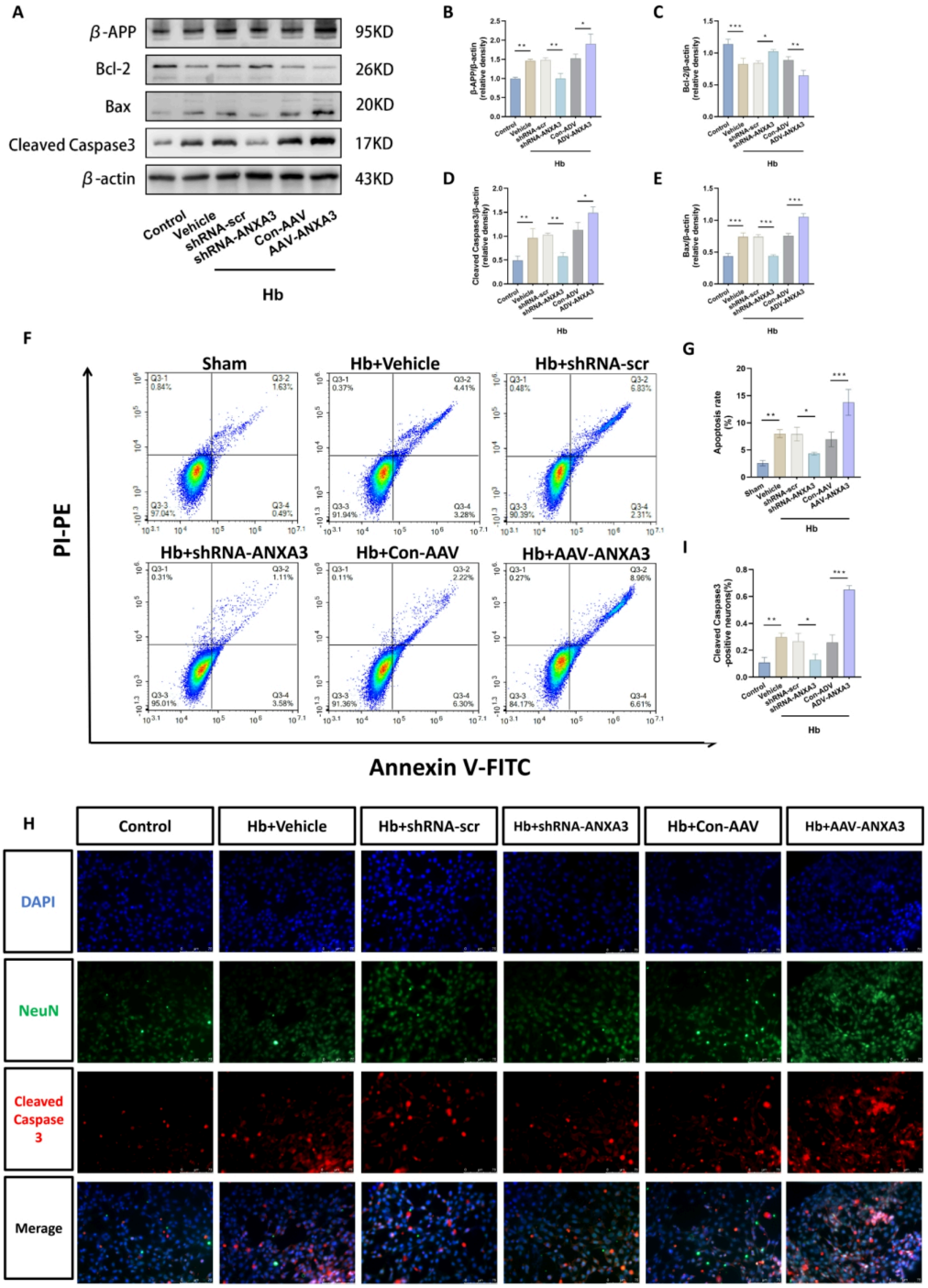


Figure 6

ANXA3 overexpression exacerbated apoptosis and axonal injury in vitro. (A–E) Representative western blot images and densitometric quantification of the expression of Bcl-2, Bax, cleaved caspase-3, and β-APP (n = 6 per group); (F–G) Representative flow cytometry images of HT22 cells; necroptosis is represented by the ratio of PI +/Annexin V+ (n = 3 per group); (H–I) Representative double-

immunofluorescence staining of cleaved caspase-3 (red) and neurons (NeuN, green) in the ipsilateral cortex. Scale bar = 75 μm. Data are shown as means ± SD. *P < 0.05, **P < 0.01, ***P < 0.001.

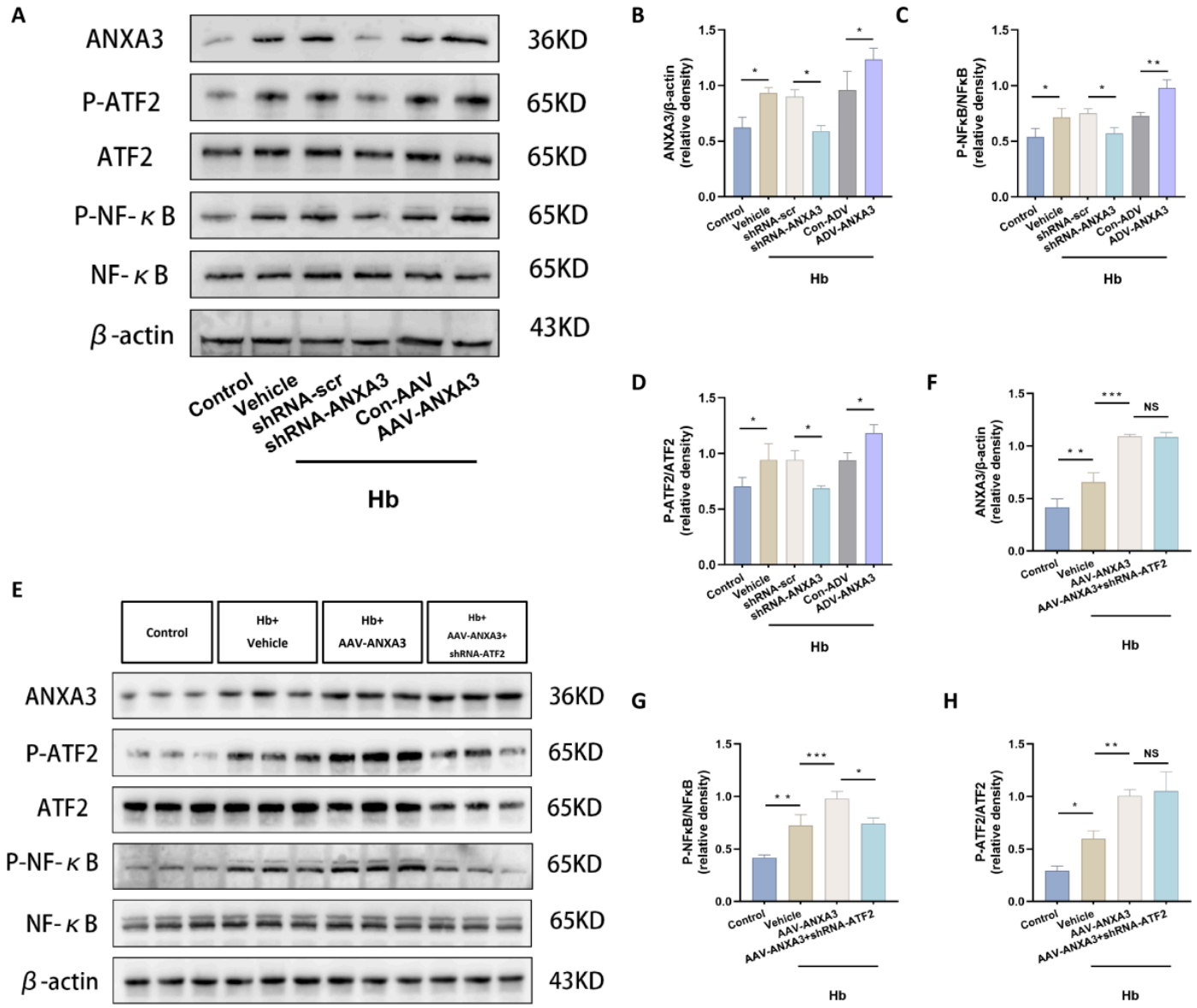


Figure 7

The ANXA3/ATF2/NF-κB signaling pathway contributes to neural injury following SAH. (A–D) Representative western blot images and densitometric quantification of the expression of ANXA3, p-ATF2, ATF2, p-NF-κB p65, and NF-κB p65 (n = 6 per group); (E–H) Further exploration of the changes in the expression levels of various molecules after ATF2 knockdown (n = 6 per group). Data are shown as means ± SD. *P < 0.05, **P < 0.01, *** P < 0.001.

Supplementary Files

This is a list of supplementary files associated with this preprint. Click to download.

- SupplementaryMaterial.docx